

Accepted Manuscript

3D-QSAR Pharmacophore Modelling, Virtual Screening and Docking Studies for Lead Discovery of a Novel Scaffold for VEGFR 2 Inhibitors: Design, Synthesis and Biological Evaluation

Mahitab K. Sobhy, Samar Mowafy, Deena S. Lasheen, Nahla A. Farag, Khaled A.M. Abouzid

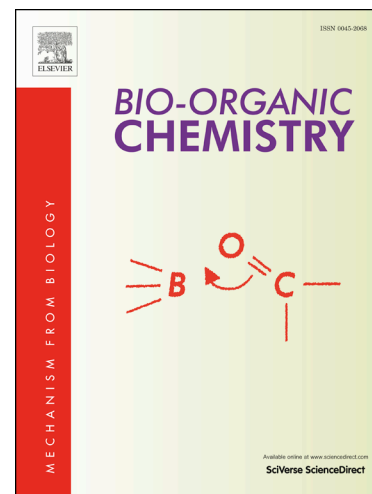
PII: S0045-2068(19)30151-8
DOI: <https://doi.org/10.1016/j.bioorg.2019.102988>
Article Number: 102988
Reference: YBIOO 102988

To appear in: *Bioorganic Chemistry*

Received Date: 29 January 2019
Revised Date: 14 May 2019
Accepted Date: 17 May 2019

Please cite this article as: M.K. Sobhy, S. Mowafy, D.S. Lasheen, N.A. Farag, K.A.M. Abouzid, 3D-QSAR Pharmacophore Modelling, Virtual Screening and Docking Studies for Lead Discovery of a Novel Scaffold for VEGFR 2 Inhibitors: Design, Synthesis and Biological Evaluation, *Bioorganic Chemistry* (2019), doi: <https://doi.org/10.1016/j.bioorg.2019.102988>

This is a PDF file of an unedited manuscript that has been accepted for publication. As a service to our customers we are providing this early version of the manuscript. The manuscript will undergo copyediting, typesetting, and review of the resulting proof before it is published in its final form. Please note that during the production process errors may be discovered which could affect the content, and all legal disclaimers that apply to the journal pertain.



Mahitab K. Sobhy^{a,*}, nahla.farag@miuegypt.edu.eg, Samar Mowafy^a, Deena S. Lasheen^b, Nahla A.

Farag^{a,*}, nahla.farag@miuegypt.edu.eg, Khaled A.M. Abouzid^{b,c}

^aPharmaceutical Chemistry Department, Faculty of Pharmacy, Misr International University, Km28 Cairo-Ismailia Road (Ahmed Orabi District), Cairo-Egypt

^bPharmaceutical Chemistry Department, Faculty of Pharmacy, Ain Shams University, Abbassia, 11566, Cairo, Egypt

^cDepartment of Organic and Medicinal Chemistry, Faculty of Pharmacy, University of Sadat City, Sadat City, Egypt

*Corresponding author.

Graphical abstract

Highlights

6,7-dihydro-5H-cyclopenta[d]pyrimidine derivatives were synthesized and biologically evaluated for their effect as VEGFR 2 inhibitors.

In order to rational new scaffold with potential VEGFR 2 inhibitory activity we perform consecutive protocols of molecular modelling.

Studying the docking result of sorafenib in the binding site of VEGFR 2.

performing 3D-QSAR pharmacophore model generation protocol to generate a valid model for virtual screening of different databases to generate new hits as VEGFR 2 inhibitors.

The structures with promising results of pharmacophore based virtual screening were then subjected to molecular docking in the binding site of VEGFR 2, docking results were analysed and filtered into 3 HITS.

The structure of the 3 HITS, along with their pharmacophore mapping and docking results were used to develop a new scaffold of VEGFR 2 inhibitors.

Abstract

A series of novel 6,7-dihydro-5H-cyclopenta[d]pyrimidine derivatives was successfully designed, synthesized and evaluated as a new chemical scaffold with vascular endothelial growth factor receptor (VEGFR 2) inhibitory activity. Compounds **6c** and **6b** showed enzyme inhibition of 97% and 87% at 10 μ M, respectively, and exhibited potent dose-related VEGFR 2 inhibition with IC₅₀ values of 0.85 μ M and 2.26 μ M, respectively. The design of the 6,7-dihydro-5H-cyclopenta[d]pyrimidine scaffold was implemented via consecutive molecular modelling protocols prior to the synthesis and biological evaluation of the derivatives. First, sorafenib was docked in the binding site of VEGFR 2 to study its binding orientation and affinity, followed by the generation of a valid 3D QSAR pharmacophore model for use in the virtual screening of different 3D databases. Structures with promising pharmacophore-based virtual screening results were refined using molecular docking studies in the binding site of VEGFR 2. A novel scaffold was designed by incorporating the results of the pharmacophore model generation and molecular docking studies. The new scaffold showed hydrophobic interactions with the kinase front pocket that may be attributed to increasing residence time in VEGFR 2, which is a key success factor for ligand optimization in drug discovery. Different derivatives of the novel scaffold were validated using

docking studies and pharmacophore mapping, where they exhibited promising results as VEGFR 2 inhibitors to be synthesized and biologically evaluated. 6,7-dihydro-5H-cyclopenta[*d*]pyrimidine is a new scaffold that can be further optimized for the synthesis of promising VEGFR 2 inhibitors.

1. Introduction

Vascular endothelial growth factor receptor (VEGFR) is a member of the receptor tyrosine kinase (RTK) family. It is essential for the growth of blood vessels, either, new (vasculogenesis) or pre-existing blood vessels (angiogenesis) [1]. VEGFR is activated by the binding of vascular endothelial growth factors (VEGFs) to its extracellular domain, causing dimerization of the receptor [2]. This conformational change makes the ATP binding site of the receptor available for ATP binding, causing phosphorylation of the tyrosine residue of the receptor and subsequent activation [2,3]. There are three subtypes of VEGFRs: VEGFR 1, 2 and 3. VEGFR 1 (Flt 1) is critical for the regulation of macrophage and monocyte migration, VEGFR 2 (KDR) is responsible for vascular endothelial cell's normal and pathological developments, and VEGFR 3 (Flt 4) is responsible for the development of lymphatic endothelial cells and the spreading of cancerous cells to lymph nodes [4]. Since VEGFR 2 is the subtype responsible for angiogenesis and vasculogenesis [3], the inhibition of VEGFR 2 will affect the blood supply to tumour cells, inhibiting their growth, proliferation and metastasis [5,6]. Inhibition of the VEGFR signalling pathway is a crucial therapeutic target for tumour inhibition. Targeting the neovascularization process of cancer cells will promote their starvation and death in a short time due to their rapid growth rate.

VEGFR small molecule inhibitors are categorized into two types according to the conformation of the receptor. Type I inhibitors compete with ATP molecules at the ATP binding site to bind to the receptor in its active form, adopting the Asp-Phe-Gly (DFG)-in conformation and consequently preventing the phosphorylation and activation of the receptor. In contrast, Type II inhibitors are non-ATP competitors that bind and stabilize the inactive form of the receptor, the DFG-out conformer, which is achieved through flipping of the DFG motif of the receptor to reveal an extra hydrophobic pocket [6,7]. Several molecules have been approved by the FDA for the treatment of different types of cancer [9]; for example, sorafenib is an oral multikinase dual-acting inhibitor that affects tumour cells directly through inhibiting the rapidly accelerated fibrosarcoma (RAF)/mitogen-activated protein kinase (MEK)/extracellular signal-regulated kinase (ERK) signalling pathway or targeting the tumour vasculature by inhibiting platelet-derived growth factor receptor-B (PDGFR-B) and VEGFR [9]. Sorafenib is a type II kinase inhibitor with a reported IC_{50} value of 0.057 μ M for PDGFR-B and 0.09 μ M for VEGFR 2 [10].

Several drug design studies were carried out with the aim of improving the potency and pharmacokinetic properties of existing VEGFR inhibitors by structural modification or finding new candidates for VEGFR inhibition. In this study, a novel 6,7-dihydro-5H-cyclopenta[*d*]pyrimidine scaffold was designed using consecutive computational protocols. The potency and effectiveness of the proposed derivatives as VEGFR 2 inhibitors were validated using molecular docking and pharmacophore mapping protocols. Then, the proposed derivatives were synthesized. Their VEGFR 2 inhibitory activity was evaluated, and their dose-related IC_{50} values were measured and compared to that of sorafenib as a reference compound.

2. Rationale

2.1. Molecular modelling studies

Computer-aided drug design (CADD) adopts different computational techniques to optimize commercially available drugs into new ligands with potential biological activities against certain

biological targets. CADD is based on quantum mechanics and molecular modelling techniques and is used to reduce the expenses and time consumed by rational drug design.

In the current study, a novel 6,7-dihydro-5H-cyclopenta[*d*]pyrimidine scaffold was designed using different molecular modelling protocols: the molecular docking of sorafenib as a potent VEGFR 2 inhibitor to understand binding affinity and orientation inside the binding site of VEGFR 2, 3D QSAR (Three Dimensional Quantitative Structure-Activity Relationship) pharmacophore model generation and virtual screening of 3D databases using Accelrys Discovery Studio software version 4.5 (DS 4.5, Accelrys Ltd., UK). The 3D QSAR pharmacophore model generation protocol builds a pharmacophore model using a set of ligands with known activity to identify the essential functional features contributing to their high potency and biological activity. The generated pharmacophore model was used for the virtual screening of three 3D databases: the DruglikeDiverse, MiniMaybridge, and scPDB databases. The selected hits of the virtual screening were analysed and subjected to molecular docking into the crystal structure of VEGFR 2 with protein data bank code 3WZE in complex with sorafenib as a reference inhibitor. The good correlation between docking scores and pharmacophore fit values provided a reliable basis for designing new VEGFR 2 inhibitors.

2.1.1. *Molecular docking of sorafenib*

A molecular docking protocol was implemented using the CDOCKER protocol under the receptor ligand interaction protocol of Accelrys Discovery Studio 4.5. CDOCKER is a grid-based molecular docking method that uses the CHARMM force field-based molecular dynamics (MD) search algorithm to dock ligands into the binding site of the receptor. Different conformations of the ligand are generated with different scoring functions, such as -CDOCKER_ENERGY (CHARMM energy of the interaction energy and ligand strain) and -CDOCKER_INTERACTION_ENERGY (interaction energy only).

The determination of the binding interactions and orientation of VEGFR 2 kinase inhibitors was studied using the X-ray crystal structure of VEGFR 2 with sorafenib (PDB code 3WZE). The molecular docking protocol (CDOCKER) of Accelrys Discovery Studio 4.5 was used, and the target protein was prepared and the active binding site identified based on the positional coordinates of the co-crystallized inhibitor. The results of the CDOCKER protocol were validated by re-docking of the co-crystallized structure of the reference sorafenib inside the active site of VEGFR 2 (PDB code 3WZE). The root mean square deviation (RMSD) between the re-docked conformer and the co-crystallized conformer of sorafenib is 0.257, (**Fig. 1**), which confirms the validity of the docking protocol.

Molecular docking simulation provides insight into the binding interaction and affinity between the compound and the receptor. Promising biological activity is indicated by lower CDOCKER energy and similar binding interactions to that of the reference co-crystallized inhibitor. A docking study of sorafenib resulted in a binding energy score of -48.92 with a total of ten hydrogen bonds. The essential amino acid Cys919 located in the hinge region binds to the nitrogen of the pyridine ring, the NH and the methyl group of the amide moiety. In addition, Glu917 in the hinge region binds to the CH proton at the 6-position of the pyridine ring; the urea moiety binds to the receptor through various hydrogen bonding interactions where both urea NH groups interact with Glu885 in the C-helix; and the carbonyl group interacts with Asp1046 in the DFG motif and with Cys1045. The fluoride atoms of the external trifluoromethyl moiety interact with His1026 and Cys1045. Furthermore, the pyridine moiety forms hydrophobic interactions with a hydrophobic pocket formed by amino acid residues Cys919, Leu1035, Ala866, Val848 and Leu840, and the phenyl ring binds to another hydrophobic pocket through interactions with Lys868, Cys1045,

Val916, Phe1047 and Val848. In addition, the terminal phenyl ring forms hydrophobic bond with Leu889, the meta trifluoromethyl substitution forms hydrophobic interactions with Val898, Ile1044, His1026 and Leu1019, and the para chloro substituent exhibits hydrophobic interactions with Leu1019 and Ile888 (**Table 4**). The resulting interactions resemble the reported binding mode of sorafenib in the X-ray crystal structure of VEGFR 2 with PDB code 3WZE [8], (**Fig. 2**).

2.1.2. 3DQ SAR pharmacophore model generation and validation

2.1.2.1. Assortment of anticancer library

A set of 25 VEGFR 2 inhibitors of known activity with IC_{50} values ranging from 0.027- 9.4 μ M were collected from the literature [11], (**Fig. 3**). Library ligands were prepared using the prepare ligands protocol of Accelrys Discovery Studio 4.5. Ligand preparation is essential for energy minimization, the correction of incorrect valences and the protonation of ligands.

2.1.2.2. 3D QSAR pharmacophore model generation

3D QSAR pharmacophore is an advanced common feature pharmacophore ligand-based protocol of Discovery Studio 4.5 that is used to explore essential pharmacophore features from a set of ligands with known activity against the biological target of interest. Pharmacophore model generation is implemented using the HypoGen algorithm [8,9], which considers only features that are common to active compounds, while common features among inactive compounds are excluded [13]. For the generation of potential pharmacophore models, a feature-mapping protocol was initiated to identify important chemical features imbedded within the training set compounds (T1-15). Subsequently, a pharmacophore model was generated using twenty-five compounds that were divided into a training set (T1-15) and a test set (S15-25), (**Fig. 3**). The features were driven by a feature-mapping protocol: hydrogen bond acceptor (HBA), hydrogen bond donor (HBD), hydrophobic (HYP) and ring aromatic (RA) features were selected, the IC_{50} of the compound was set as the activity property of the model, the uncertainty property was changed from the default value of 3.0 to 1.5, and validation was set as true with maximum omitted features of zero. Accordingly, ten predictive pharmacophore model hypotheses were generated and validated.

2.1.2.3. Validation of pharmacophore models

The HypoGen algorithm generates different hypotheses, and the best-generated hypothesis is chosen according to different parameters. The cost difference is calculated from the null cost and the total cost of each hypothesis, where the total cost is the summation of three components: weight, error and configuration cost. The weight component increases in a Gaussian form as the feature weight deviates from an ideal value (2.0); the error component increases as the root mean squared (RMS) difference between the estimated and experimental activities for the training set compounds increases; and the configuration component is a constant cost that depends on the hypothesis space being optimized. The fixed cost and null cost are another two theoretical costs that are measured by the algorithm, where the fixed cost is the minimum possible cost of a model that fits all the data perfectly, and the null cost is the maximum cost of a model devoid of any features. For the model to be statistically significant, the difference between the null and fixed cost must be greater than that between the total and fixed cost, and to generate a statistically reliable model above 90%; the

difference between the null and total cost should be greater than or equal to 70 bits [14]. Accordingly, the best generated hypothesis is the model with the highest cost difference.

The generated pharmacophore model is validated by the measurement of its statistical significance and its ability to estimate the biological activity of new compounds. Model validation depends on the cost difference, accuracy of the predicted activity of the training set compounds compared to their experimental activity, and mapping of sorafenib on the generated model as a reference standard. Ten 3D QSAR pharmacophore models were generated with at least three chemical features each (**Table 1**). Hypothesis 1 is the most statistically significant hypothesis among the ten generated pharmacophore model hypotheses, and it has five features: one hydrogen bond acceptor (HBA), three hydrophobic (HYP), and one ring aromatic (RA) (**Fig. 4**). Accordingly, hypothesis 1 has the highest cost difference of 140.98, indicating a predictive power above 90%, with the lowest (RMS) of 1.03 reflecting a high correlation between predicted and experimental activity and a high correlation coefficient of 0.975 corresponding to the ability of the model to predict the activity of the training set compounds (**Table 2**).

2.1.2.4. Pharmacophore mapping of sorafenib

The generated pharmacophore model was further validated by mapping an active reference compound, sorafenib, into the generated model using the ligand mapping protocol of Accelrys Discovery Studio 4.5 and scored a fit value of 6.19 (**Fig. 5**).

2.1.3. Virtual screening

Virtual screening is the adoption of computational techniques to identify potentially active compounds from existing databases or virtual libraries. The screening was carried out using the search and edit 3D database protocol of Accelrys Discovery Studio 4.5. Three 3D databases, DruglikeDiverse, MiniMaybridge, and scPDB, containing a total of 12,930 compounds were mapped into the generated pharmacophore model. The mapping of the three databases resulted in 2370 compounds with the features of the validated pharmacophore model (hypothesis 1). The best-matched compounds were filtered and selected according to their fit values into 136 compounds with fit values higher than that of sorafenib.

2.1.4. Docking studies of virtually screened compounds

The docking results of the 136 compounds of the pharmacophore-based virtual screening were ranked according to their binding affinity and binding mode. The top three hits were **KM10259**, **CDI665171** and **2r4b_GW7**. **KM10259** has a fit value of 7.19 and the highest docking score of -42.28. The urea NH groups form two hydrogen bonds with Glu885, and the urea carbonyl group forms two hydrogen bonds with Cys1045 and Asp1046. In addition, hydrophobic interactions occur between the furan ring and a hydrophobic pocket formed by residues Val848, Leu1035, Ala866 and Cys919, between the terminal phenyl ring and Leu889, and the para chloro substituent interacts with Leu1019, Ile1044 and Val898 (**Table 3**).

The docking score of **CDI665171** is -33.81, its fit value is 7.80, and it binds to the receptor through hydrogen bonds similar to those of **KM10259**. Its hydrophobic interactions involve the binding of the terminal methyl group to residues Leu1035, Cys919, Phe918 and Leu840, the binding of the thiazole ring to residues Leu1035, Cys1045, Val916, Val848 and Ala866 and the interaction of the phenyl ring attached to the thiazole ring with Lys868, Cys1045, Val899 and

Val916. In addition, hydrophobic interactions between the terminal phenyl ring and the Leu889 amino acid were observed (**Table 3**).

2r4b_GW7, with a fit value of 7.10 and a CDOCKER binding score of -35.08, binds to the receptor through interaction of the N1 of the pyrimidine ring with Cys919 in the hinge region and binding of the CH proton at the 2-position of the pyrimidine ring with Glu917. Cys919 and Glu917 are key amino acids for the hydrogen bonding of the adenine ring of ATP to the hinge region of VEGFR 2 [15]. The hydrophobic interactions of **2r4b_GW7** involve the binding of the thienyl ring to the kinase front pocket formed by residues Phe918, Leu840, Leu1035 and Ala866 and the hydrophobic binding of the pyrimidine ring to residues Leu1035, Cys919 and Ala866. In addition, the phenyl ring binds to Val916, Cys1045, Val848, Phe1047 and Lys868, the 3-chloro substituent of the phenyl ring forms hydrophobic interactions with Lys868 and Val916, and the terminal phenyl ring forms hydrophobic interactions with Leu889 (**Table 3**). The three hits showed consistency in rendering the interactions of VEGFR 2 inhibitors.

2.2. Design strategy

In studying the structure-activity relationship of reported VEGFR 2 inhibitors and analysing their binding modes, three main features of type II inhibitors of VEGFR 2 were reported: most inhibitors include a flat heteroaromatic ring system that binds to the NH of Cys919 in the hinge region; a hydrogen bond donor and acceptor pair, which can be a urea or an amide group that binds with Glu885 and Asp1046 in the enzyme DFG motif, where two hydrogen bonds are formed between NH of the urea or amide group and Glu885 and another hydrogen bond is between the CO group and Asp1046 [16]; and finally, the binding of the terminal aryl group in the newly created allosteric hydrophobic pocket exposed upon flipping of the DFG loop, as shown in the inactive conformation or DFG-out conformation of the enzyme [17].

Compound **2r4b_GW7** has a fit value of 7.10 and exhibits the 5 features (1HBA, 3HYP and 1RA) of the validated pharmacophore model, while sorafenib has a fit value of 6.19 and exhibits only 4 features (1HBA, 3HYP), (**Table 4**). Molecular docking studies of the hit compound **2r4b_GW7** revealed a hydrogen bond between N1 of the thienyl pyrimidine moiety and Cys919 and a hydrogen bond between the CH proton at the 2-position of the pyrimidine ring and Glu917. Both Cys919 and Glu917 are key amino acids for the hydrogen bonding of ATP to the hinge region of VEGFR 2 [15]. The thienyl pyrimidine moiety forms additional hydrophobic interactions at the front pocket of the kinase domain with residues Leu840, Ala866, Phe918 and Leu1035, (**Table 4**). Hydrophobic interaction with the kinase front pocket complements the hydrogen bonding with the hinge region, increasing the residence time [8], which is a key factor in improving potency *in vivo* and enhancing the correlation between the *in vitro* and *in vivo* efficacy of drugs [18].

Utilizing the aforementioned essential structural features, bioisosteric modification strategies and the results of the 3D QSAR pharmacophore model generation and molecular modelling protocols, a proposed scaffold of 6,7-dihydro-5H-cyclopenta[*d*]pyrimidine derivatives was designed and synthesized. The design of the new scaffold was based on the replacement of the N-methylpicolinamide moiety of sorafenib with a 6,7-dihydro-5H-cyclopenta[*d*]pyrimidine moiety. Bioisosteric replacement was carried out by the substitution of the oxygen linker with a classical NH bioisostere, (**Fig. 6**). Introducing new substituents at different positions of an aromatic ring of a hit compound may optimize the binding affinity of the drug with the receptor in addition to conferring the physicochemical properties essential for drug distribution and metabolism. Different derivatives of (**I**) were proposed with alternative lipophilic substituents at the terminal aromatic ring

to occupy the hydrophobic allosteric pocket. Substituents were either electron withdrawing, such as chloro and trifluoromethyl groups, or electron donating, such as methyl and methoxy groups.

2.2.1. Validation of the proposed scaffold of VEGFR 2 inhibitors

2.2.1.1. Pharmacophore mapping of the proposed VEGFR 2 inhibitors

The activity of the proposed scaffold as an effective VEGFR 2 inhibitor was validated through mapping of the proposed derivatives into the validated pharmacophore model. The results showed that the proposed derivatives **6a**, **6b**, **6c**, **6d** and **6e** exhibited five features of the generated pharmacophore model with fit values ranging from 6.63 to 9.21 (**Table 5**), which are higher than that of the reference compound sorafenib, at 6.19.

2.2.1.2. Docking of the proposed derivatives of VEGFR 2 inhibitors

Molecular docking of the proposed derivatives is essential for the assessment of binding affinity and binding interactions with key residues at the active binding site of VEGFR 2. The proposed derivatives **6a-6e** were docked inside the binding site of VEGFR 2 with PDB code 3WZE with a similar binding mode. The N1 of the cyclopentapyrimidine ring forms two hydrogen bonds with Phe918 and Cys919 at the hinge region, and the CH proton at the 2-position of the pyrimidine ring forms a hydrogen bond with Glu917 at the hinge region. In addition, both urea NH groups interact with Glu885 in the C-helix, and the carbonyl group of the urea moiety interacts with Asp1046 and Cys1045 (**Table 5**). Moreover, compound **6e** forms two additional hydrogen bonds due to the interaction of the fluoride atoms of the terminal trifluoromethyl with His1026 and Cys1045. Furthermore, the pyrimidine moiety forms hydrophobic interactions with a hydrophobic pocket consisting of residues Cys919, Leu1035 and Ala866, and the phenyl ring binds to another hydrophobic pocket through interactions with amino acids Lys868, Cys1045, Val916, Phe 1047 and Val848. In addition, the terminal phenyl ring interacts hydrophobically with Leu889, and the substituents of the terminal phenyl ring interact with different amino acids according to the type and position of the substituent. The hydrophobic interactions of the proposed derivatives are similar to those of the reference compound except for an additional hydrophobic interaction between the cyclopentane moiety and the entrance region of the adenine binding site. The cyclopentane moiety in derivatives **6a** and **6e** also forms additional hydrophobic interactions with Leu1035 and Leu840, while compounds **6b**, **6c** and **6d** bind with Leu1035, Leu840 and Phe918. Hydrophobic interaction at the kinase entrance region might prolong the residence time and improve the binding kinetics of VEGFR 2 receptor [18], (**Fig. 7, Table 5**).

3. Results and discussion

3.1. Chemistry

The synthetic route of the key intermediates and final compounds of the proposed scaffold is illustrated in Schemes 1 and 2, respectively. The synthesis of the key intermediates (**2a-e**) was carried out by reacting p-nitroaniline with different isocyanates in dry dichloromethane for 48 hours at room temperature [19] to give compounds (**1a-e**), followed by the reduction of 4-nitrophenyl substituted phenyl ureas (**1a-e**) using Pd/C in methanol [20] to give the corresponding amino derivatives (**2a-e**).

The synthesis of the 6,7-dihydro-5H-cyclopenta[*d*]pyrimidine derivatives (**6a-e**) was achieved through multistep reactions starting with a one-step Thorpe-Ziegler cyclization by reacting adiponitrile and sodium hydride in toluene [21] to give 2-aminocyclopent-1-ene carbonitrile **3**, which was then cyclized by heating under reflux with formic acid and acetic anhydride for 48 hours

[22] to provide the 6,7-dihydro-5H-cyclopenta[*d*] pyrimidinone derivative **4**. The chlorination of **4** was carried out by heating with phosphorus oxychloride [23]. The key intermediates (**2a-e**) were then coupled with the chloro derivative **5** to give the corresponding 6,7-dihydro-5H-cyclopenta[*d*] pyrimidine derivatives (**6a-e**), and the reaction was followed up using TLC.

3.2. *Biological analysis*

Initial screening of all synthesized final compounds was carried out at a single dose of 10 μM to evaluate their inhibitory activity against VEGFR 2 kinase. The percentage inhibition of 6,7-dihydro-5H-cyclopenta[*d*]pyrimidine derivatives **6b** and **6c** was 87% and 97%, respectively. The enzymatic activity of the other synthesized compounds ranged from weak to moderate inhibition. Compounds **6d** and **6e** showed low inhibition despite their promising molecular modelling results due to their poor solubility in DMSO (**Table 7**).

The inhibitory effect of the synthesized compounds on VEGFR 2 revealed that the unsubstituted terminal phenyl ring in **6a** resulted in weak enzyme inhibition. However, the addition of different substituents, especially at the meta position of the terminal phenyl ring, resulted in a higher enzyme inhibitory effect [4], as shown in compounds **6b** and **6c** due to the addition of the 3-Cl-4-CH₃ and 4-Cl-3-CF₃ substituents. In addition, **6b** and **6c** exhibited high docking scores of -34.28 and -29.29, respectively, and high pharmacophore mapping fit values of 6.63 for compound **6b** and 9.21 for compound **6c**. Synthesized compounds with high percentage inhibition (above 80%) against VEGFR 2 were subjected to five-dose testing to determine their IC₅₀ value, and values of 2.26 μM and 0.85 μM were obtained for compounds **6b** and **6c**, respectively (**Table 8**).

4. Conclusion

In summary, a novel VEGFR 2 inhibitor scaffold was designed using several molecular modelling protocols. A valid 3D QSAR pharmacophore model was generated, followed by pharmacophore-based virtual screening of three different databases. Virtually screened compounds were filtered by docking into the VEGFR 2 structure with PDB code 3WZE. According to the results of molecular docking studies, a new scaffold of VEGFR 2 was designed based on substitution of the N-methylpicolinamide moiety of sorafenib with 6,7-dihydro-5H-cyclopenta[*d*]pyrimidine.

Five different derivatives of the proposed scaffold were tested for validation using pharmacophore mapping and molecular docking protocols. The proposed derivatives resulted in fit values, binding energies and binding interactions that are comparable to those of sorafenib. Following the molecular modelling results, the five proposed structures were synthesized and subjected to biological evaluation against the VEGFR 2 enzyme. Compounds **6b** and **6c** exhibited high percentage inhibition of 87% and 97%, respectively, at 10 μM . The compounds with the highest enzyme inhibitory effect were tested for VEGFR 2 inhibition and demonstrated IC₅₀ values in the sub-micromolar range. The IC₅₀ values of compounds **6c** and **6b** were 0.85 μM and 2.26 μM , respectively. Therefore, compounds **6c** and **6b** represent a new molecular scaffold that can be further optimized and used for the design of promising potent VEGFR 2 inhibitors.

5. Experimental

Starting material and reagents were purchased from Sigma Aldrich or Alfa-Aeser organics and were used without further purification. Melting points were recorded using BUCHI B-540 apparatus and were uncorrected. Reactions were monitored using thin layer chromatography (TLC) purchased from Merck and performed on 0.255 mm silica gel plates, with visualization under U.V. light (254 nm). The hydrogenation process was carried out using hydrogenator (Parr Shaker) apparatus. FT-IR spectra were recorded on a Perkin Elmer FT-IR spectrophotometer and ^1H NMR spectra were recorded on BRUCKER 400 MHz spectrophotometer at Ain Shams University. Mass spectra were recorded on Thermo Scientific ISQ LT gas chromatograph mass spectrometer at the regional center for Mycology and Biotechnology Al-Azhar University and on thermos Q-exactive orbitrap instrument at laboratory for single cell mass spectrometry, quantitative biology center, Japan.

5.1. Chemistry

5.1.1. General procedure for the preparation of compounds (**1a–e**)

A solution of p-nitroaniline (1 g, 6 mmol: 1 equiv.) in dry dichloromethane (20 mL), was stirred with the appropriate isocyanate (6 mmol: 1 equiv.) at room temperature for 48 hours. The resulting mixture was filtered and the filtered solid was crystallized from ethanol to yield derivatives (**1a–e**) [19].

5.1.1.1. 1-(4-Nitrophenyl)-3-phenylurea (**1a**)

Yield 40% as yellowish white crystals, m.p 226-228 °C, (as reported) [24].

5.1.1.2. 1-(3-Chloro-4-methylphenyl)-3-(4-nitrophenyl)urea (**1b**)

Yield 50% as yellow orange crystals, m.p 182-185 °C, (as reported) [10].

5.1.1.3. 1-(3-trifluoromethyl-4-chlorophenyl)-3-(4-nitrophenyl)urea (**1c**)

Yield 90% as pale yellow crystals, m.p 238-240 °C. FT-IR (ν max, cm^{-1}): 1596 (C=C), 1646 (C=N), 1717 (C=O), 3128 (CH aromatic), 3352 (NH).

5.1.1.4. 1-(3-Methoxyphenyl)-3-(4-nitrophenyl)urea (**1d**)

Yield 47% as yellow crystals, m.p 210-212 °C, (as reported) [24].

5.1.1.5. 1-(4-Nitrophenyl)-3-(3-(trifluoromethyl)phenyl)urea (**1e**)

Yield 60% as greenish yellow crystals, m.p 260 °C. FT-IR (ν max, cm^{-1}): 1575 (C=C), 1621 (C=N), 1720 (C=O), 3162 (CH aromatic), 3356 (NH).

5.1.2. General procedure for the preparation of compounds (**2a–e**)

Pd-C (0.1 g, 10%) was added to a solution of the appropriate nitro phenyl urea derivative (**1a–e**) (4 mmol) in methanol (100 ml), the mixture was stirred under H_2 at room temperature, at 60 bar for 4 hours. The catalyst was removed by filtration over celite. Then the filtrate was concentrated and dried to afford crystals of compounds (**2a–e**) which were then recrystallized from methanol [20].

5.1.2.1. 1-(4-Aminophenyl)-3-phenylurea (**2a**)

Yield 70% as white crystals, m.p 224-227 °C, (as reported) [25].

5.1.2.2. 1-(4-Aminophenyl)-3-(3-Chloro-4-methylphenyl)urea (**2b**)

Yield 80% as grey crystals, m.p 203-205 °C, (as reported) [10].

5.1.2.3. 1-(4-Aminophenyl)-3-(3-trifluoromethyl-4-chlorophenyl)urea (**2c**)

Yield 80% as grayish white crystals, m.p 187-190 °C. ¹H NMR (400 MHz, DMSO-*d*₆) δ 6.52-6.54 (d, *J* = 8 Hz, 1H, H_{2'}), 7.07-7.09 (d, *J* = 8 Hz, 1H, H_{6'}), 7.58-7.60 (d, *J* = 8 Hz, 1H, H_{5''}), 7.67-7.71 (m, 2H, H_{3'}, H_{5'}), 8.10-8.12 (d, *J* = 8 Hz, 1H, H_{6''}), 8.19-8.31 (m, 1H, H_{2''}), 8.99 (s, 1H, NH, exchangeable by D₂O), 9.37 (s, 1H, NH, exchangeable by D₂O), 9.44 (s, 1H, NH, exchangeable by D₂O), 9.64 (s, 1H, NH, exchangeable by D₂O). Ms: (Mwt.: 329): m/z, 331 [M⁺⁺², (30%)], 329 [M⁺, (100%)], 108 (77%), 80 (40%), 53 (24%).

5.1.2.4. 1-(4-Aminophenyl)-3-(3-Methoxyphenyl)urea (**2d**)

Yield 70% as white crystals, m.p 165-168 °C, (as reported) [10].

5.1.2.5. 1-(4-Aminophenyl)-3-(3-(trifluoromethyl)phenyl)urea (**2e**)

Yield 80% as grayish white crystals, m.p 147-149 °C. ¹H NMR (400 MHz, DMSO-*d*₆) δ 4.80 (s, 2H, NH, exchangeable by D₂O), 6.51-6.53 (d, *J* = 8 Hz, 2H, H_{2'}, H_{6'}), 7.07-7.1 (d, *J* = 12 Hz, 2H, H_{3'}, H_{5'}), 7.25-7.27 (d, *J* = 8 Hz, 1H, H_{4''}), 7.46-7.54 (m, 1H, H_{5''}), 7.48-7.50 (d, *J* = 8 Hz, 1H, H_{6''}), 8.01 (s, 1H, H_{2''}), 8.27 (s, 1H, NH, exchangeable by D₂O), 8.88 (s, 1H, NH, exchangeable by D₂O). Ms: (Mwt.: 295): m/z, 296 [M⁺⁺¹, (18%)], 295 [M⁺, (93%)], 108 (100%), 80 (55%), 53 (22%).

5.1.3. 2-aminocyclopent-1-ene carbonitrile (**3**)

A solution of adipodinitrile (10.8 g, 100 mmol) in toluene (100 ml) is added dropwise to a slurry of sodium hydride (60% suspension in oil, 4.20 g, 105 mmol) in anhydrous toluene (30 ml). The mixture was heated under reflux for 15 hours. The product was extracted with ethyl acetate (3x50 ml). Then recrystallized by dissolving in hot toluene (25 ml) and then adding petroleum ether (150 ml). The product was obtained as yellowish white solid (6.60 g, 61%), m.p 148 °C [21].

5.1.4. 6,7-dihydro-3H-cyclopenta[*d*]pyrimidin-4(5H)-one (**4**)

Acetic anhydride (46 mL, 492.38 mmol: 23.8 equiv.) was added portion wise to a stirred formic acid (23 mL, 614.92 mmol: 29.8 equiv.) at 0 °C over 30 minutes. This was followed by addition of compound (**3**) (2 g, 20 mmol: 1 equiv.) and stirring under reflux at 130 °C for 48 hours. The solvent was evaporated under vacuum and the resultant solid was washed with diethyl ether, dried and recrystallized from methanol. The product was separated as buff crystals (1.2 g, 60%), m.p 220 °C [26].

5.1.5. 4-chloro-6,7-dihydro-5H-cyclopenta[*d*]pyrimidine (**5**)

A mixture of compound (**4**) (2 g, 0.01 mmol: 1 equiv.) and phosphorous oxychloride (29 mL, 278 mmol: 18.2 equiv.) was heated under reflux for 3 hours. The mixture was then slowly poured on ice/water, neutralized using ammonia solution (33%, 50 mL), then extracted with ethyl acetate (2x50 mL). The combined organic layer was separated and the solvent was evaporated under vacuum to afford brown solid that was washed with diethyl ether to give the titled compound (**5**) as brown crystals (1.5 g, 76%) which was used directly in the next reaction [27].

5.1.6. General procedure for the preparation of compounds (**6a–e**)

The appropriate 4-aminophenyl substituted phenyl urea (**2a-e**) (1 mmol: 1 equiv.) and TEA (0.3 mL, 2 mmol: 2 equiv.) were added to a solution of the 4-chloro cyclopenta[*d*]pyrimidine derivative **5** (0.25 g, 1 mmol: 1 equiv.) in ethanol (15 mL). The mixture was heated under reflux for 18–24 hours and the reaction was followed up using TLC. The resultant solid was collected by filtration, washed with hot ethanol, allowed to dry and recrystallized from ethanol to give the titled compounds (**6a-e**).

*5.1.6.1. 1-(4-(6,7-dihydro-5H-cyclopenta[*d*]pyrimidin-4-ylamino)phenyl)-3-phenylurea (6a)*

The product was separated as yellowish brown powder (0.2 g, 33%), m.p > 300 °C. ¹H NMR (400 MHz, DMSO-*d*₆) δ 1.16-1.20 (t, 2H, cyclopentenyl H), 1.94-1.99 (m, 1H, cyclopentenyl H), 2.63-2.65 (m, 1H, cyclopentenyl H), 2.72-2.77 (m, 1H, cyclopentenyl H), 3.07-3.11 (m, 1H, cyclopentenyl H), 6.51-6.53 (d, *J* = 8 Hz, 2H, H_{2'}, H_{6'}), 6.90-7.01 (m, 1H, H_{4''}), 7.08-7.10 (d, *J* = 8 Hz, 2H, H_{3'}, H_{5'}), 7.22-7.47 (m, 4H, H_{2''}, H_{3''}, H_{5''}, H_{6''}), 8.32 (s, 1H, pyrimidine H), 8.41 (s, 1H, NH, exchangeable by D₂O), 8.66 (s, 1H, NH, exchangeable by D₂O), 8.90 (s, 1H, NH, exchangeable by D₂O). HRMS (ESI-MS) calcd: 346.16339 for C₂₀H₁₉N₅O [M + H⁺]. Found: 346.16672.

*5.1.6.2. 1-(3-chloro-4-methylphenyl)-3-(4-(6,7-dihydro-5H-cyclopenta[*d*]pyrimidin-4-ylamino)phenyl)urea (6b)*

The product was separated as yellowish brown powder (0.102 g, 17%), m.p 233-235 °C. ¹H NMR (400 MHz, DMSO-*d*₆) δ 1.09-1.13 (m, 1H, cyclopentenyl H), 1.86-1.91 (m, 1H, cyclopentenyl H), 2.04-2.12 (m, 1H, cyclopentenyl H), 2.26 (s, 3H, Ph-CH₃), 2.76-2.83 (m, 3H, cyclopentenyl H), 6.55-6.56 (d, 2H, H_{2'}, H_{6'}), 7.00-7.58 (m, 5H, ArH), 8.37 (s, 1H, pyrimidine H), 8.68 (s, 1H, NH, exchangeable by D₂O), 8.70 (s, 1H, NH, exchangeable by D₂O), 8.81 (s, 1H, NH, exchangeable by D₂O). HRMS (ESI-MS) calcd: 394.14333 for C₂₁H₂₀N₅OCl [M + H⁺]. Found: 394.14331.

*5.1.6.3. 1-(4-chloro-3-(trifluoromethyl)phenyl)-3-(4-(6,7-dihydro-5H-cyclopenta[*d*]pyrimidin-4-ylamino)phenyl)urea (6c)*

The product was separated as yellow powder (0.11 g, 19%), m.p 288-290 °C. ¹H NMR (400 MHz, DMSO-*d*₆) δ 1.22 (s, 1H, cyclopentenyl H), 1.98-2.06 (m, 2H, cyclopentenyl H), 2.76-2.79 (m, 3H, cyclopentenyl H), 7.29 (s, 1H, ArH), 7.40-7.42 (d, *J* = 8 Hz, 1H, H_{5''}), 7.57-7.61 (m, 4H, ArH), 7.64-7.66 (d, *J* = 8 Hz, 1H, H_{6''}), 8.15 (s, 1H, pyrimidine H), 8.71 (s, 1H, NH, exchangeable by D₂O), 9.37 (s, 1H, NH, exchangeable by D₂O), 9.94 (s, 1H, NH, exchangeable by D₂O). HRMS (ESI-MS) calcd: 448.11507 for C₂₁H₁₇N₅OClF₃ [M + H⁺]. Found: 448.11562.

*5.1.6.4. 1-(4-(6,7-dihydro-5H-cyclopenta[*d*]pyrimidin-4-ylamino)phenyl)-3-(3-methoxyphenyl)urea (6d)*

The product was separated as grayish white powder (0.13 g, 22%), m.p >300 °C. ¹H NMR (400 MHz, DMSO-*d*₆) δ 1.24 (s, 4H, cyclopentenyl H), 1.91 (s, 2H, cyclopentenyl H), 3.50 (s, 3H, OCH₃, below water of DMSO), 6.86-6.88 (d, *J* = 8 Hz, 1H, H_{2'}), 6.96-6.97 (d, *J* = 4 Hz, 1H, H_{6'}), 7.04-7.06 (d, *J* = 8 Hz, 1H, H_{4''}), 7.21-7.23 (d, *J* = 8 Hz, 1H, H_{3'}), 7.47-7.50 (d, *J* = 12 Hz, 1H, H_{6''}), 7.62-7.65 (d, *J* = 12 Hz, 1H, H_{5''}), 7.82-7.86 (d, 1H, H_{2''}), 7.93-7.94 (d, *J* = 4 Hz, 1H, H_{5'}), 8.15 (s, 1H, pyrimidine H), 8.65 (s, 1H, NH, exchangeable by D₂O), 8.67 (s, 1H, NH, exchangeable by D₂O), 10.56 (s, 1H, NH, exchangeable by D₂O); HRMS (ESI-MS) calcd: 376.17721 for C₂₁H₂₂N₅O₂ [M + H⁺]. Found: 376.17709.

5.1.6.5.1-(4-(6,7-dihydro-5H-cyclopenta[d]pyrimidin-4-ylamino)phenyl)-3-(3-(trifluoromethyl)phenyl)urea (**6e**)

The product was separated as grayish white powder (0.13 g, 22%), m.p 283-285 °C. ¹H NMR (400 MHz, DMSO-*d*₆) δ 1.14 (s, 4H, cyclopentenyl H), 1.24 (s, 2H, cyclopentenyl H), 6.50-6.52 (d, *J* = 8 Hz, 2H, H_{2'}, H_{6'}), 7.08-7.10 (d, *J* = 8Hz, 2H, H_{4''}, H_{5''}), 7.22-7.24 (d, *J* = 8Hz, 2H, H_{3'}, H_{5'}), 7.46-7.48 (d, *J* = 8 Hz, 1H, H_{6''}), 7.57 (s, 1H, H_{2''}), 7.99 (s, 1H, pyrimidine H), 9.01 (s, 1H, NH, exchangeable by D₂O), 8.84 (s, 1H, NH, exchangeable by D₂O), 10.56 (s, 1H, NH, exchangeable by D₂O). HRMS (ESI-MS) calcd: 414.15404 for C₂₁H₁₉N₅O₃ [M + H⁺]. Found: 294.08449 and 370.08269.

5.2. Biology

The structures of the synthesized compounds were submitted to BPS Bioscience, San Diego, CA, USA (www.bpsbioscience.com) for a VEGFR 2 tyrosine kinase assay. The assay was carried out using a Kinase-Glo Plus Luminescence Kinase Assay Kit (Promega). Kinase activity is measured by quantitating the amount of ATP remaining in the solution after a kinase reaction. The luminescent signal from the assay is correlated with the amount of ATP present and is inversely correlated with the amount of kinase activity. Compounds **6a**, **6b**, **6c**, **6d**, and **6e** were diluted in 10% DMSO, and 5 μl of the dilution was added to a 50 μl reaction so that the final concentration of DMSO was 1% in all reactions.

All of the enzymatic reactions were conducted at 30 °C for 45 minutes. The 50 μl reaction mixture contained 40 mM Tris, pH 7.4, 10 mM MgCl₂, 0.1 mg/ml BSA, 1 mM DTT, 0.2 mg/ml Poly (Glu, Tyr) substrate, 10 μM ATP and enzyme. After the enzymatic reaction, 50 μl of Kinase-Glo Plus Luminescence Kinase Assay Solution (Promega) was added to each reaction, and the plate was incubated for 15 minutes at room temperature. The luminescence signal was measured using a BioTek Synergy 2 microplate reader.

References

- [1] C.S. Abhinand, R. Raju, S.J. Soumya, P.S. Arya, P.R. Sudhakaran, VEGF-A/VEGFR2 signaling network in endothelial cells relevant to angiogenesis, *J. Cell Commun. Signal.* 10 (2016) 347–354.
- [2] F. Musumeci, M. Radi, C. Brullo, S. Schenone, Vascular Endothelial Growth Factor (VEGF) Receptors: Drugs and New Inhibitors, *J. Med. Chem.* 55 (2012) 10797–10822.
- [3] V.A. Machado, D. Peixoto, R. Costa, H.J.C. Froufe, R.C. Calhelha, R.M. V Abreu, I.C.F.R. Ferreira, R. Soares, M.R.P. Queiroz, Synthesis, antiangiogenesis evaluation and molecular docking studies of 1-aryl-3-[(thieno[3,2-b]pyridin-7-ylthio)phenyl]ureas: Discovery of a new substitution pattern for type II VEGFR-2 Tyr kinase inhibitor, *Bioorg. Med. Chem.* 23 (2015) 6497–6509.
- [4] J.E. Daniel S. La, Julie Belzile, James V. Bready, Angela Coxon, Thomas DeMelfi, Nicholas Doerr, A.M.L. Julie C. Flynn, Shaun R. Flynn, Russell F. Graceffa, Shawn P. Harriman, Jay F. Larrow, M.M.W. Matthew W. Martin, Michael J. Morrison, Vinod F. Patel, Philip M. Roveto, Ling Wang, J.-C.H. Douglas A. Whittington, Yohannes Teffera, Zhiyang Zhao, Anthony J. Polverino, Novel 2,3-Dihydro-1,4-Benzoxazines as Potent and Orally Bioavailable Inhibitors of Tumor-Driven Angiogenesis, *J. Med. Chem.* 51 (2008) 1695–1705.
- [5] M. Rajagopalan, S. Balasubramanian, A. Ramaswamy, P. Prakash Mathur, Pharmacophore based 3D-QSAR modeling and free energy analysis of VEGFR-2 inhibitors, *J. Enzyme Inhib. Med.*

- Chem. 28 (2013) 1236–1246.
- [6] N.M.Y. Elsayed, R.A.T. Serya, M.F. Tolba, M. Ahmed, K. Barakat, D.A. Abou El Ella, K.A.M. Abouzid, Design, synthesis, biological evaluation and dynamics simulation of indazole derivatives with antiangiogenic and antiproliferative anticancer activity, *Bioorg. Chem.* 82 (2019) 340–359.
- [7] M.I. Shahin, D.A. Abou, E. Ella, N.S.M. Ismail, K.A.M. Abouzid, Design, synthesis and biological evaluation of type-II VEGFR-2 inhibitors based on quinoxaline scaffold, *Bioorg. Chem.* 56 (2014) 16–26.
- [8] K. Okamoto, M. Ikemori-Kawada, A. Jestel, K. Von König, Y. Funahashi, T. Matsushima, A. Tsuruoka, A. Inoue, J. Matsui, Distinct binding mode of multikinase inhibitor lenvatinib revealed by biochemical characterization, *ACS Med. Chem. Lett.* 6 (2015) 89–94.
- [9] V.E. Kwitkowski, T.M. Prowell, A. Ibrahim, A.T. Farrell, R. Justice, S.S. Mitchell, R. Sridhara, R. Pazdur, FDA Approval Summary: Temeirolimus as Treatment for Advanced Renal Cell Carcinoma, *Oncologist.* 15 (2010) 428–435.
- [10] M.A. Aziz, R.A.T. Serya, D.S. Lasheen, A.K. Abdel-az, A. Esmat, A.M. Mansour, A.N.B. Singab, K.A.M. Abouzid, Discovery of Potent VEGFR-2 Inhibitors based on Furopyrimidine and Thienopyrimidine Scaffolds as Cancer Targeting Agents, *Sci. Rep.* 6 (2016) 24460.
- [11] Y. Oguro, N. Miyamoto, K. Okada, T. Takagi, H. Iwata, Y. Awazu, H. Miki, A. Hori, K. Kamiyama, S. Imamura, Design, synthesis, and evaluation of 5-methyl-4-phenoxy-5H-pyrrolo-[3,2-d]pyrimidine derivatives: Novel VEGFR2 kinase inhibitors binding to inactive kinase conformation, *Bioorg. Med. Chem.* 18 (2010) 7260–7273.
- [12] W.Y.C. Chen, P.Y. Chen, C.Y.C. Chen, J.G. Chung, Exploring 3D-QSAR Pharmacophore Mapping of Azaphenanthrene derivatives for mPGES-1 inhibition Using HypoGen Technique, in: 2008 IEEE Symp. Comput. Intell. Bioinforma. Comput. Biol., 2008: pp. 207–213.
- [13] L. H, S. J, H. R, HypoGen: An Automated System for Generating Predictive 3D Pharmacophore Models, *Pharmacophore Perception, Dev. Use Drug Des.* 2 (2000) 171–187.
- [14] S. Sakkiah, S. Thangapandian, S. John, Y. Jung, K. Woo, 3D QSAR pharmacophore based virtual screening and molecular docking for identification of potential HSP90 inhibitors, *Eur. J. Med. Chem.* 45 (2010) 2132–2140.
- [15] K. Sanphanya, S. Phowichit, S.K. Wattanapitayakul, V. V. Fokin, O. Vajragupta, Novel VEGFR-2 kinase inhibitor identified by the back-to-front approach, *Bioorg Med Chem Lett.* 23 (2013) 2962–2967.
- [16] A. Ghith, K.M. Youssef, N.S.M. Ismail, K.A.M. Abouzid, Design, synthesis and molecular modeling study of certain VEGFR-2 inhibitors based on thienopyrimidine scaffold as cancer targeting agents, *Bioorg. Chem.* 83 (2019) 111–128.
- [17] J. Dietrich, C. Hulme, L.H. Hurley, The design, synthesis, and evaluation of 8 hybrid DFG-out allosteric kinase inhibitors: A structural analysis of the binding interactions of Gleevec®, Nexavar®, and BIRB-796, *Bioorganic Med. Chem.* 18 (2010) 5738–5748.
- [18] E. V Schneider, J. Böttcher, R. Huber, K. Maskos, L. Neumann, Structure – kinetic relationship study of CDK8 / CycC specific compounds, *PNAS.* 110 (2013) 8081–8086.
- [19] Y. Dai, K. Hartandi, Z. Ji, A.A. Ahmed, D.H. Albert, J.L. Bauch, J.J. Bouska, P.F. Bousquet, G.A. Cunha, K.B. Glaser, C.M. Harris, D. Hickman, J. Guo, J. Li, P.A. Marcotte, K.C. Marsh, M.D. Moskey, R.L. Martin, A.M. Olson, D.J. Osterling, L.J. Pease, N.B. Soni, K.D. Stewart, V.S. Stoll, P. Tapang, D.R. Reuter, S.K. Davidsen, M.R. Michaelides, Discovery of N-(4-(3-Amino-1H-indazol-4-yl)phenyl)-N'-(2-fluoro-5-methylphenyl)urea (ABT-869), a 3-Aminoindazole-Based Orally Active Multitargeted Receptor Tyrosine Kinase Inhibitor, *J. Med. Chem.* 50 (2007) 1584–1597.
- [20] T. Suzuki, M.N.A. Khan, H. Sawada, E. Imai, Y. Itoh, K. Yamatsuta, N. Tokuda, J. Takeuchi, T. Seko, H. Nakagawa, N. Miyata, Design, Synthesis, and Biological Activity of a Novel Series of

- Human Sirtuin-2-Selective Inhibitors, *J. Med. Chem.* 55 (2012) 5760–5773.
- [21] Y. Nurlela, A.J. Minnaard, S. Achmad, D. Wahyuningrum, A Long Chain Alcohol as Support in Solid Phase Organic Synthesis, *Sains Malaysiana.* 40 (2011) 977–983.
- [22] M.S. Coumar, M.T. Tsai, C.Y. Chu, B.J. Uang, W.H. Lin, C.Y. Chang, T.Y. Chang, J.S. Leou, C.H. Teng, J.S. Wu, M.Y. Fang, C.H. Chen, J.T.A. Hsu, S.Y. Wu, Y.S. Chao, H.P. Hsieh, Identification, SAR studies, and X-ray Co-crystallographic analysis of a novel furanopyrimidine aurora kinase a inhibitor, *ChemMedChem.* 5 (2010) 255–267.
- [23] J.I. Pyo, S.H. Lee, C.S. Cheong, A facile synthesis of some substituted furopyrimidine derivatives, *J. Heterocycl. Chem.* 43 (2006) 1129–1133.
- [24] L.S. Reddy, S.K. Chandran, S. George, N.J. Babu, A. Nangia, Crystal Structures of N-Aryl-N'-4-Nitrophenyl Ureas: Molecular Conformation and Weak Interactions Direct the Strong Hydrogen Bond Synthons, *Cryst. Growth Des.* 7 (2007) 2675–2690.
- [25] M. Uno, H.S. Ban, W. Nabeyama, H. Nakamura, De novo Design and synthesis of N-benzylanilines as new candidates for VEGFR tyrosine kinase inhibitors, *Org. Biomol. Chem.* 6 (2008) 979–981.
- [26] A. Gangjee, Y. Zhao, S. Raghavan, C.C. Rohena, S.L. Mooberry, E. Hamel, Structure–Activity Relationship and in Vitro and in Vivo Evaluation of the Potent Cytotoxic Anti-microtubule Agent N-(4-Methoxyphenyl)-N,2,6-trimethyl-6,7-dihydro-5H-cyclopenta[d]pyrimidin-4-aminium Chloride and Its Analogues As Antitumor Agents, *J. Med. Chem.* 56 (2013) 6829–6844.
- [27] M. Adel, R.A.T. Serya, D.S. Lasheen, K.A.M. Abouzid, Identification of new pyrrolo[2,3-d]pyrimidines as potent VEGFR-2 tyrosine kinase inhibitors: Design, synthesis, biological evaluation and molecular modeling, *Bioorg. Chem.* 81 (2018) 612–629.

Fig. 1. 3D image of the superimposition of the re-docked conformer of sorafenib over the co-crystallized conformer (colored yellow) with RMSD value of 0.257. (For interpretation using colors, the reader is referred to the web version of this article).

Fig. 2. [A] The reported 2D image of binding interactions of sorafenib in the x-ray crystal structure of VEGFR 2 with PDB code 3WZE [8], [B] 3D image of sorafenib inside 3WZE using Accelrys Discovery Studio 4.5; docking score is -48.92 along with the hydrogen and hydrophobic interaction with the key residues of the receptor. (For interpretation using colors, the reader is referred to the web version of this article).

Fig. 3. The library of T1-15 training set and S15-25 test set of known active VEGFR 2 inhibitors used for pharmacophore model generation along with their IC₅₀ values (μM) indicated in parenthesis.

Fig. 4. The best generated Pharmacophore model with three features: hydrogen bond acceptor (HBA) colored green, ring aromatic (RA) colored orange and hydrophobic (HYP) colored cyan. With their inter-feature distances in angstroms and angles displayed.

Fig. 5. Sorafenib as reference compound mapped into the best pharmacophore model with fit value of 6.19.

Fig. 6. Illustration of binding of sorafenib and the proposed scaffold (**I**) to the binding regions of VEGFR 2.

Fig. 7. 2D image of hydrogen bonds and hydrophobic interactions of sorafenib and proposed derivatives **6a** and **6d** with the kinase domain of VEGFR 2.

Scheme 1. Synthesis of 4-aminophenyl substituted phenyl ureas reagents and conditions: (a) Phenyl isocyanates, DCM, rt, 48 hrs; (b) H₂, Pd/C, MeOH, rt, 4 hrs.

Scheme 2. Synthesis of 6,7-dihydro-5H-cyclopenta[d]pyrimidine derivatives reagents and conditions: (a) NaH, toluene, 15 hrs; (b) HCOOH, acetic anhydride, reflux, 48 hrs; (c) POCl₃, reflux, 3 hrs; (d) Ethanol, TEA, reflux, 18-48 hrs.

Table 1. Tabular column illustrating the details of the ten hypotheses generated using hypoGen algorithm.

Hypothesis	Total cost	Cost difference	RMS	Correlation coefficient	Features ^b	Maximum fit
1	59.35	140.98	1.03	0.97	HBA, HYP, HYP, HYP, RA	10.80
2	66.56	133.78	1.42	0.95	HBA, HYP, HYP, HYP	7.36
3	74.56	125.78	1.76	0.92	HBD, HYP, HYP, HYP	7.81
4	74.86	125.48	1.77	0.92	HBD, HYP, HYP, HYP	7.90
5	74.95	125.39	1.76	0.92	HYP, HYP, HYP, HYP, HYP	8.83
6	75.82	124.52	1.74	0.92	HBA, HBA, HYP, HYP, HYP	7.08
7	76.17	124.16	1.78	0.92	HBA, HBD, HYP, RA	6.23
8	76.54	123.80	1.80	0.92	HBD, HYP, HYP, HYP	6.39
9	78.23	122.10	1.89	0.91	HBA, HYP, HYP, RA	7.34
10	78.97	121.37	1.89	0.91	HBD, HYP, RA, RA	6.41

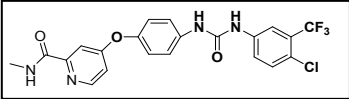
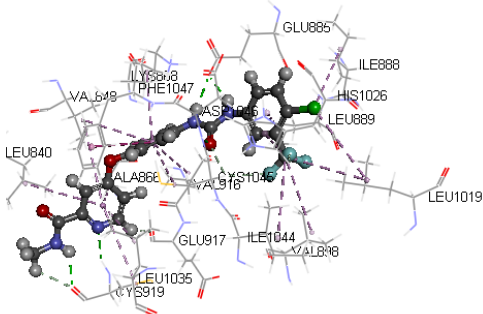
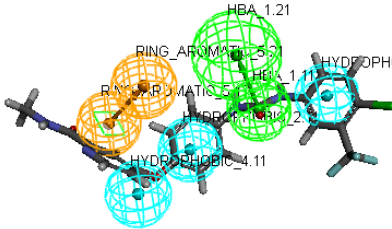
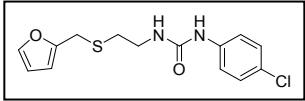
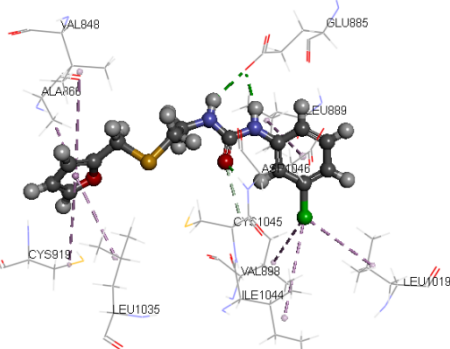
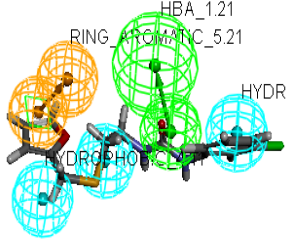
^babbreviations used for features; hydrogen bond acceptor (HBA), hydrophobic (HYP) and ring aromatic (RA).

Table 2. The experimental and predicted activity values of the training set compounds according to hypothesis 1 along with their fit values.

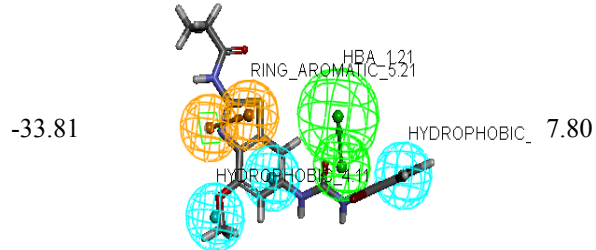
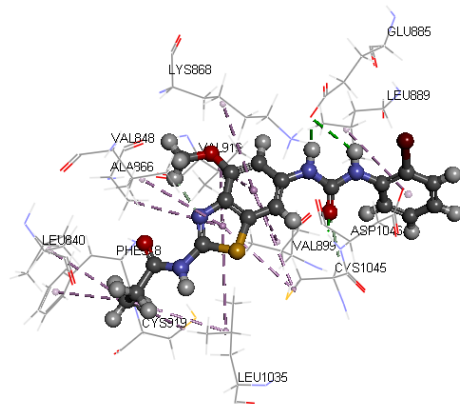
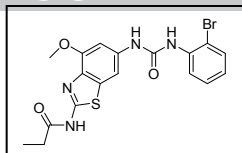
Training set	Experimental activity IC ₅₀ nM	Predicted activity IC ₅₀ nM	Fit value
T1	940	688.787	6.505
T2	870	1,299	6.230
T3	340	349.804	6.800
T4	4.1	8.839	8.397
T5	32	13.729	8.206
T6	5.3	5.586	8.596
T7	4.4	8.998	8.389

T8	19	12.989	8.230
T9	2.7	3.086	8.854
T10	33	33.111	7.823
T11	110	113.757	7.287
T12	7.1	7.335	8.478
T13	30	14.713	8.176
T14	3.7	3.033	8.861
T15	14	17.234	8.107

Table 3. Docking score, hydrogen and hydrophobic interactions of sorafenib and the three top hits with VEGFR 2 (pdb code 3WZE), along with their pharmacophore mapping and fit values inside the best-generated pharmacophore model.

Compound	Binding interactions	CDOCKER energy	Pharmacophore mapping	Fit value
Sorafenib	 	-48.92		6.19
KM10259	 	-42.28		7.16

CDI665171



2r4b_GW7

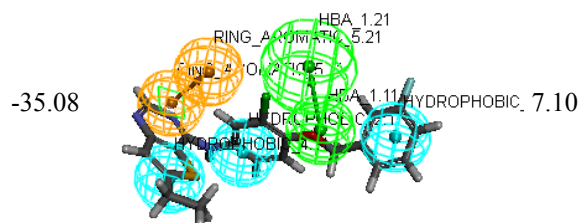
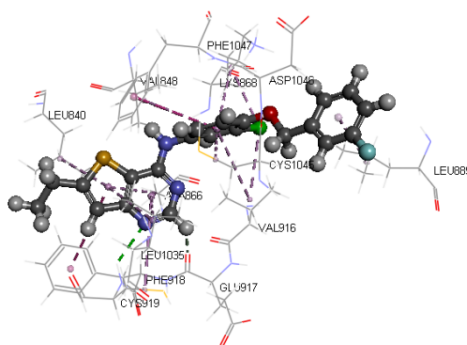
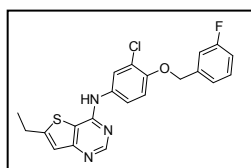


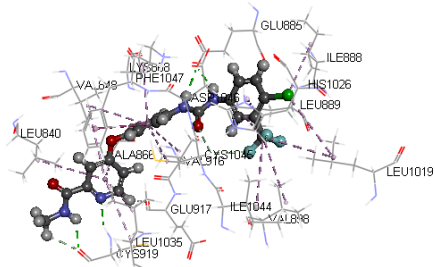
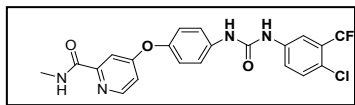
Table 4. Docking results of sorafenib and the three top hits **KM10259**, **CDI665171** and **2r4b_GW7** in the active site of VEGFR 2 (3WZE) showing hydrogen bonds and hydrophobic interactions.

fx1

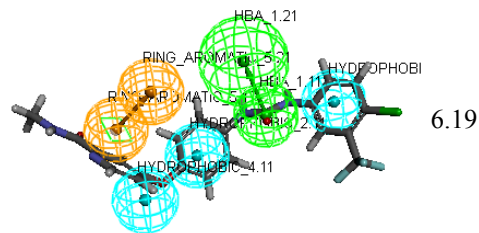
Table 5. Docking score, hydrogen bonds and hydrophobic interactions of sorafenib and the proposed derivatives with VEGFR 2 (pdb code 3WZE), along with their pharmacophore mapping and fit values inside the best generated pharmacophore model.

Compound	interactions	CDOCKER energy	Pharmacophore mapping	Fit value
----------	--------------	----------------	-----------------------	-----------

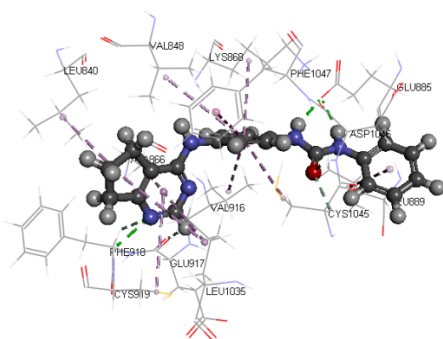
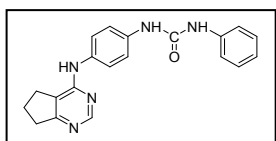
Sorafenib



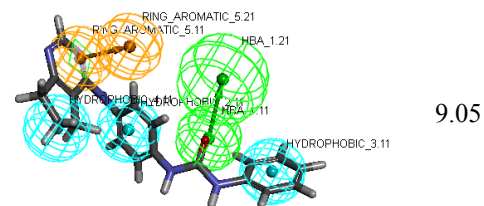
-48.92



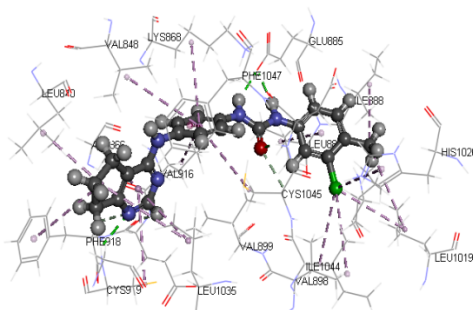
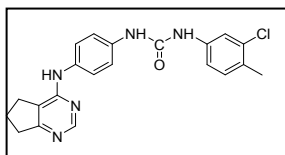
6a



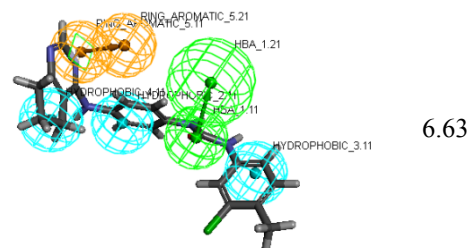
-29.49



6b



-34.28



6e

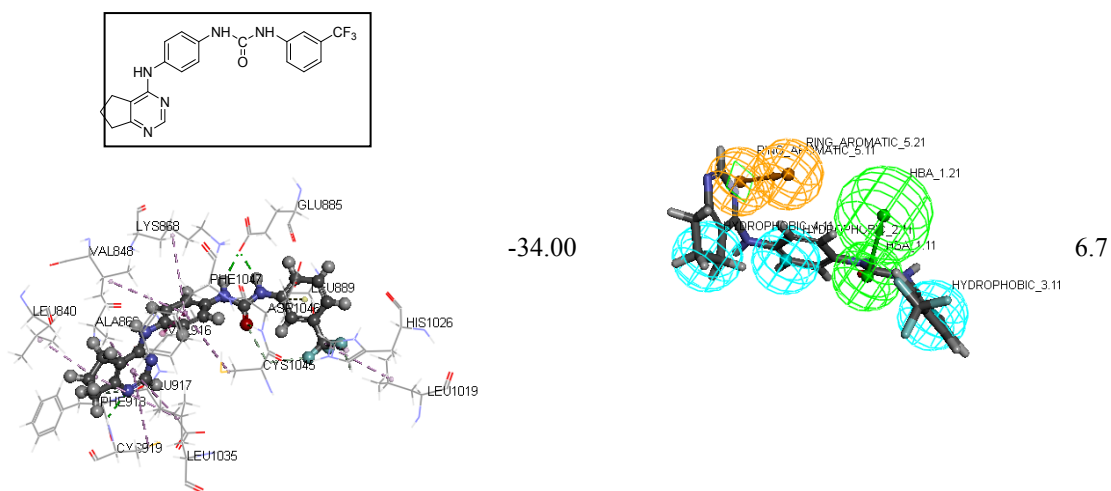


Table 6. Docking results of sorafenib and the three top hits **KM10259**, **CDI665171** and **2r4b_GW7** in the active site of VEGFR 2 (3WZE) showing hydrogen bonds and hydrophobic interactions.

fx2

Table 7. VEGFR 2 enzyme inhibition of the synthesized compounds at 10 μ M.

Compounds	R	% inhibition
6a	H	5
6b	3-Cl-4-CH ₃	87
6c	4-Cl-3-CF ₃	97
6d*	3-OCH ₃	0
6e*	3- CF ₃	1

*these compounds are sparingly dissolved at 10mM in 100% DMSO.

Table 8. The IC₅₀ value of Synthesized compounds with high VEGFR 2 percent inhibition.

Compounds	VEGFR 2 IC ₅₀ (μ M)
6b	2.26
6c	0.85
Staurosporine	0.09
Sorafenib	0.09